

Reduced density matrices and entanglement entropy in free lattice models

Ingo Peschel¹ and Viktor Eisler²

¹ Fachbereich Physik, Freie Universität Berlin, Arnimallee 14, D-14195 Berlin, Germany

² Niels Bohr Institute, University of Copenhagen, Blegdamsvej 17, DK-2100 Copenhagen Ø, Denmark

Abstract. We review the properties of reduced density matrices for free fermionic or bosonic many-particle systems in their ground state. Their basic feature is that they have a thermal form and thus lead to a quasi-thermodynamic problem with a certain free-particle Hamiltonian. We discuss the derivation of this result, the character of the Hamiltonian and its eigenstates, the single-particle spectra and the full spectra, the resulting entanglement and in particular the entanglement entropy. This is done for various one- and two-dimensional situations, including also the evolution after global or local quenches.

1. Introduction

Reduced density matrices contain the information on some part of a quantum system and are a basic tool in many-body physics. The ones commonly employed describe the properties of one or two selected *particles* in a many-particle system and allow to calculate important physical quantities like the total energy or the density correlations. These reduced density matrices (RDM's) were first introduced by Dirac [1] and studied already in the 1930's, see e.g. [2, 3]. In the usual terminology, they are just the static one- and two-particle correlation functions.

The RDM's we want to discuss here are of a different type and refer to a different question. They arise if one divides a system in *space*, or, more generally, in Hilbert space, and asks how the two parts are coupled in the given wave function. This corresponds to the analysis by Schrödinger in 1935 [4] when he introduced the concept of entanglement. The general form of this coupling is given by the Schmidt decomposition which displays all entanglement features in a simple and transparent way. To obtain it in a specific case, one needs the RDM's for the two *regions* in question.

The present interest in this problem, although it had also been a theme in quantum optics, arose in the beginning of the nineties in two seemingly disconnected areas, in the theory of black holes [5, 6, 7] and in the numerical investigation of quantum chains [8, 9]. In both cases, the motivation came from the wish to consider some subsystem which

is in contact with its environment. For the quantum chains, this led to the density-matrix renormalization group (DMRG) which can treat large systems with spectacular accuracy and revolutionized the field [10, 11]. A third input then came from the area of quantum information, where the structure of quantum states also plays a central role. This resulted in particular in a renewed and extensive study of the entanglement entropy [12, 13, 14] which is a simple and convenient measure of the entanglement and follows directly from the RDM eigenvalues.

The purpose of this article is to give a coherent account of the reduced density matrices just described for a class of models where they can be obtained in closed form. These are free fermions including the related spin chains and free bosons in the form of coupled oscillators. They will be considered either in their ground state or in certain other pure quantum states. In this case, the RDM's are found to have a Boltzmann-like form with a certain free-particle operator in the exponent. The problem is thereby reduced to the study of this associated Hamiltonian and its characteristic features. The main property of interest is the eigenvalue spectrum since it determines the spectrum of the RDM itself and thus the entanglement properties, in particular the entanglement entropy. Both the spectra and the entropies will be presented for a variety of different situations. The problem on a lattice is very clear-cut. The partitioning is done by selecting two sets of discrete sites and there are no divergencies for finite sizes. On the other hand, there is only a small number of analytical results and one has to invoke numerics frequently. Lattice systems are also required for the DMRG, and the initial motivation for the studies was to understand the performance of this intriguing numerical method by looking at solvable models.

In section 2 we will provide some background on entanglement, the Schmidt decomposition and the RDM's. Then, in section 3, we give the general form of the reduced density matrices for free fermions or bosons and discuss the methods for obtaining them. For quantum chains, this also contains relations to two-dimensional classical models. In section 4 we show the eigenvalue spectra for various one- and two-dimensional systems and discuss their typical appearance, their scaling behaviour and the change with the dimension. The characteristics of the single-particle eigenfunctions, the nature of the effective Hamiltonian and some further aspects are the topics of section 5. In section 6 we turn to the entanglement entropy and summarize the important results with emphasis on their relation to the spectra. Finally, in section 7, we review the temporal behaviour of the entanglement after different types of quenches. The material is drawn preferentially from our own studies and some of it also appeared in a recent book [15]. However, the scope is different here and a considerable number of figures were prepared exclusively for this review.

2. Background

In this section, we summarize the basic features of entangled states and reduced density matrices in order to create the frame for the results to be presented later. For more

details, see e.g. the short review [16].

2.1. Schmidt decomposition

Consider a quantum system which is divided into two distinct parts 1 and 2. Then a state $|\Psi\rangle$ of the total system can be written

$$|\Psi\rangle = \sum_{m,n} A_{m,n} |\Psi_m^1\rangle |\Psi_n^2\rangle \quad (1)$$

where $|\Psi_m^1\rangle$ and $|\Psi_n^2\rangle$ are orthonormal basis functions in the two Hilbert spaces. But a rectangular matrix \mathbf{A} can always be written in the form \mathbf{UDV}' where \mathbf{U} is unitary, \mathbf{D} is diagonal and the rows of \mathbf{V}' are orthonormal. This is called the singular-value decomposition and similar to the principal-axis transformation of a symmetric square matrix [17]. Using this in (1) and forming new bases by combining the $|\Psi_m^1\rangle$ with \mathbf{U} and the $|\Psi_n^2\rangle$ with \mathbf{V}' , one obtains the Schmidt decomposition [18]

$$|\Psi\rangle = \sum_n \lambda_n |\Phi_n^1\rangle |\Phi_n^2\rangle \quad (2)$$

which gives the total wave function as a single sum of products of orthonormal functions. Here the number of terms is limited by the smaller of the two Hilbert spaces and the weight factors λ_n are the elements of the diagonal matrix \mathbf{D} . If $|\Psi\rangle$ is normalized, their absolute magnitudes squared sum to one. The entanglement properties are encoded in the set of λ_n . Only if all except one are zero, the sum reduces to a single term and $|\Psi\rangle$ is a product state, i.e. non-entangled. In all other cases a certain entanglement is present and if all λ_n are equal in size, one would call the state maximally entangled. Of course, this refers to a particular bipartition and one should investigate different partitions to obtain a complete picture.

2.2. Reduced density matrices

The entanglement structure just discussed can also be found from the density matrices associated with the state $|\Psi\rangle$. This is, in fact, the standard way to obtain it. Starting from the total density matrix

$$\rho = |\Psi\rangle\langle\Psi| \quad (3)$$

one can, for a chosen division, take the trace over the degrees of freedom in one part of the system. This gives the reduced density matrix for the other part, i.e.

$$\rho_1 = \text{tr}_2(\rho) \quad , \quad \rho_2 = \text{tr}_1(\rho) \quad (4)$$

These hermitian operators can be used to calculate arbitrary expectation values in the subsystems. Moreover, it follows from (2) that their diagonal forms are

$$\rho_\alpha = \sum_n |\lambda_n|^2 |\Phi_n^\alpha\rangle\langle\Phi_n^\alpha| \quad , \quad \alpha = 1, 2 \quad (5)$$

This means that

- ρ_1 and ρ_2 have the same non-zero eigenvalues
- these eigenvalues are given by $w_n = |\lambda_n|^2$

Therefore the eigenvalue spectrum of the ρ_α gives directly the weights in the Schmidt decomposition and a glance at this spectrum shows the basic entanglement features of the state, for the chosen bipartition. For this reason, it has also been termed “entanglement spectrum” recently [19]. One also sees that the $|\Phi_n^\alpha\rangle$ appearing in (2) are the eigenfunctions of the ρ_α . For the single-particle RDM’s mentioned in the introduction, these eigenfunctions are known as “natural orbitals” in quantum chemistry [20].

In the DMRG algorithm, these properties are used to truncate the Hilbert space by calculating the ρ_α , selecting the m states $|\Phi_n^\alpha\rangle$ with largest weights w_n and deleting the rest. This procedure is expected to work well if the total weight of the discarded states is sufficiently small. Therefore the form of the density-matrix spectra is decisive for the success of the method.

It is interesting that Schmidt himself already worked with the RDM’s. Studying coupled linear integral equations, he derived a spectral representation of the form (2) for an unsymmetric kernel K in terms of the eigenfunctions of the two symmetric operators KK' and $K'K$. His paper (which is based on his doctoral thesis with Hilbert) also contains the recipe for the best approximation as it is used in the DMRG.

2.3. Entanglement entropy

Whereas the full RDM spectra give the clearest impression of the entanglement in a bipartite system, it is also desirable to have a simple measure which condenses this information into one number. This can be achieved by generalizing the usual (von Neumann) entropy definition to reduced density matrices. The entanglement entropy therefore reads:

$$S_1 = -\text{tr}(\rho_1 \ln \rho_1) = -\sum_n w_n \ln w_n, \quad (6)$$

where the trace has been rewritten as a sum using the eigenvalues w_n . The most important properties are as follows.

- The entropy is determined purely by the spectrum of ρ_1 , which is known to be identical to the spectrum of ρ_2 . Therefore $S_1 = S_2$ holds for arbitrary bipartitions and one can simply write S and talk of *the* entanglement entropy.
- The entropy vanishes for product states, and has a maximal value of $S = \ln M$ if one has M non-zero eigenvalues which are all equal, $w_n = 1/M$ for $n = 1, 2, \dots, M$. Using this, one can write in general $S = \ln M_{\text{eff}}$, thereby defining an effective number of states coupled in parts 1 and 2. This gives a simple interpretation to S .

Although there are other entanglement measures [21], the entropy is the standard one for bipartitions and will be discussed in detail later. It is important to keep in mind that it measures a *mutual connection* and will, in general, not be proportional to the size of a subsystem.

3. RDM's for free lattice models

3.1. Systems

In the following we consider models with a Hamiltonian which is quadratic in either fermion or boson operators and thus can be diagonalized by a Bogoliubov transformation. In principle, these can be quite general, but we will concentrate on the following physically important systems

- Fermionic hopping models with conserved particle number and Hamiltonian

$$H = -\frac{1}{2} \sum_{\langle m,n \rangle} t_{m,n} c_m^\dagger c_n \quad (7)$$

where the symbol $\langle \rangle$ denotes nearest neighbours. Apart from homogeneous systems we will consider dimerized chains, where $t_{n,n+1}$ alternates between $1 \pm \delta$, and the case of single defects.

- Coupled oscillators with eigenfrequency ω_0 and Hamiltonian

$$H = \sum_n \left[-\frac{1}{2} \frac{\partial^2}{\partial x_n^2} + \frac{1}{2} \omega_0^2 x_n^2 \right] + \frac{1}{4} \sum_{\langle m,n \rangle} k_{m,n} (x_m - x_n)^2 \quad (8)$$

These are systems with an optical spectrum and bosonic pair creation and annihilation.

- Spin one-half chains which are equivalent to free fermions via the Jordan-Wigner transformation. The most general one is the XY chain with a Z field, described by

$$H = - \sum_n \left[\frac{1+\gamma}{2} \sigma_n^x \sigma_{n+1}^x + \frac{1-\gamma}{2} \sigma_n^y \sigma_{n+1}^y \right] - h \sum_n \sigma_n^z \quad (9)$$

where the σ_n^α are Pauli matrices at site n . For $\gamma = 0$ this reduces to the XX model, corresponds to (7) with nearest-neighbour hopping and can also model hard-core bosons. For $\gamma \neq 0$, it contains pair creation and annihilation terms. For $\gamma = 1$ it becomes the Ising model in a transverse field (TI model) which we write, in a slightly different notation

$$H = - \sum_n \sigma_n^z - \lambda \sum_n \sigma_n^x \sigma_{n+1}^x, \quad (10)$$

The solubility of the models in itself does not yet mean that the RDM's are easily accessible. For example, they have been considered in the critical XXZ spin chain, but the formulae are very complicated, see [22, 23]. The free lattice models, however, have eigenstates with special properties which permit to make a simple general statement.

3.2. General result

For these free-particle models, the reduced density matrices for the ground state can be written

$$\rho_\alpha = \frac{1}{Z} e^{-\mathcal{H}_\alpha}, \quad \mathcal{H}_\alpha = \sum_{l=1}^L \varepsilon_l f_l^\dagger f_l \quad (11)$$

Here L is the number of sites in subsystem α and the operators f_l^\dagger, f_l are fermionic or bosonic creation and annihilation operators for single-particle states with eigenvalues ε_l . The f 's are related to the original operators in the subsystem by a canonical transformation. Thus ρ_α has the form of a thermal density matrix with an effective Hamiltonian \mathcal{H}_α which is of the same free-particle type as H . In (11) it is already given in diagonal form. The constant Z , written in analogy to thermodynamics, ensures the correct normalization $\text{tr}(\rho_\alpha) = 1$.

This form of ρ_α is rather suggestive since one has a similar situation as for a system in contact with a thermal bath. However, no assumption about the relative sizes of the two coupled systems enters here. More importantly, the operator \mathcal{H}_α is *not* the Hamiltonian H restricted to the subsystem α . Therefore (11) is not a true Boltzmann formula. Nevertheless, the problem has been reduced to the study of a certain Hamiltonian and its thermodynamic properties. The features of \mathcal{H}_α will be the topic of the next chapters. Generally, one can say that it corresponds to an inhomogeneous system even if the subsystem it describes is homogeneous. This will be seen in more detail in section 5.2. Here we first discuss how one arrives at (11). These considerations will also show that validity of (11) goes even beyond the ground state.

3.3. Methods

Basically, there are three methods to obtain the reduced density matrices.

(I) Integration over part of the variables according to the definition (4). This can be done e.g. for N coupled harmonic oscillators [24, 25]. In this case the ground state is a Gaussian in the normal coordinates, provided no normal frequency vanishes. In terms of the original coordinates x_n of the oscillators, it has the form

$$\Psi(x_1, x_2, \dots, x_N) = C \exp\left(-\frac{1}{2} \sum_{m,n}^N A_{m,n} x_m x_n\right) \quad (12)$$

Here C is a normalization constant and the matrix \mathcal{A} is the square root $\mathcal{V}^{1/2}$ of the dynamical matrix associated with the potential energy. By forming ρ and integrating out e.g. the variables x_{L+1}, \dots, x_N one obtains $\rho_1(x_1, x_2, \dots, x_L | x'_1, x'_2, \dots, x'_L)$ which is again a Gaussian. With proper linear combinations y_l of the coordinates, it contains only squares $y_l^2, y_l'^2$ and differences $(y_l - y_l')^2$. Early treatments worked with this integral operator [5, 6]. However, one can convert the differences into second derivatives and thereby obtain the differential operator

$$\rho_1 = K \prod_{l=1}^L \exp\left(-\frac{1}{4}\omega_l^2 y_l^2\right) \exp\left(\frac{1}{2} \frac{\partial^2}{\partial y_l^2}\right) \exp\left(-\frac{1}{4}\omega_l^2 y_l'^2\right) \quad (13)$$

where the exponents become quadratic expressions in terms of boson operators. A diagonalization then gives the single exponential (11) with \mathcal{H}_1 describing a collection of L new harmonic oscillators. Their eigenfrequencies ε_l follow from \mathcal{A} by dividing it into

the submatrices a^{11} , a^{12} , a^{21} , and a^{22} , according to whether the sites are in part 1 or in part 2. Then the $L \times L$ matrix $a^{11}(a^{11} - a^{12}(a^{22})^{-1}a^{21})^{-1}$ has the eigenvalues $\coth^2(\varepsilon_l/2)$.

If $L = 1$, there is just one such oscillator with a frequency ε which differs from ω_0 . Its eigenstates have a different spatial extent and may therefore be called ‘‘squeezed’’. For $N = 2$ the resulting Schmidt decomposition of $\Psi(x_1, x_2)$ in terms of these states can easily be written down and is well known, see e.g. [26, 27].

The method can also be used for systems of non-interacting fermions. In this case one first has to write the ground state in exponential form and then use Grassmann variables for the integration [28, 29].

(II) Via correlation functions [30, 12, 31]. The simplest case is a system of free electrons hopping on N lattice sites in a state described by a Slater determinant. In such a state, all many-particle correlation functions factorize into products of one-particle functions. For example,

$$\langle c_m^\dagger c_n^\dagger c_k c_l \rangle = \langle c_m^\dagger c_l \rangle \langle c_n^\dagger c_k \rangle - \langle c_m^\dagger c_k \rangle \langle c_n^\dagger c_l \rangle \quad (14)$$

If all sites are in the same subsystem, a calculation using the reduced density matrix must give the same result. This is guaranteed by Wick’s theorem if ρ_α is the exponential of a free-fermion operator

$$\rho_\alpha = K \exp\left(-\sum_{i,j=1}^L h_{i,j} c_i^\dagger c_j\right) \quad (15)$$

where i and j are sites in the subsystem. With the form of ρ_α fixed, the hopping matrix $h_{i,j}$ is then determined such that it gives the correct one-particle correlation functions $C_{i,j} = \langle c_i^\dagger c_j \rangle$. The two matrices are diagonalized by the same transformation and one finds (see also [29])

$$\mathbf{h} = \ln [(\mathbf{1} - \mathbf{C})/\mathbf{C}] \quad (16)$$

The same formula also relates the eigenvalues ε_l and ζ_l of \mathbf{h} and \mathbf{C} . Expressed differently, the ε_l follow from the equation

$$(\mathbf{1} - 2\mathbf{C}) \phi_l = \tanh\left(\frac{\varepsilon_l}{2}\right) \phi_l. \quad (17)$$

If there is pair creation and annihilation, one has to include the ‘anomalous’ correlation functions $F_{i,j} = \langle c_i^\dagger c_j^\dagger \rangle$ and $F_{i,j}^* = \langle c_j c_i \rangle$. To reproduce them, the operator \mathcal{H}_α then must also contain pair terms. Diagonalizing it in the usual way [32], one finds that the single-particle eigenvalues follow from two coupled equations, which can be combined into a single one. For real \mathbf{F} this reads

$$(2\mathbf{C} - \mathbf{1} - 2\mathbf{F})(2\mathbf{C} - \mathbf{1} + 2\mathbf{F}) \phi_l = \tanh^2\left(\frac{\varepsilon_l}{2}\right) \phi_l. \quad (18)$$

and reduces to the previous result (17) if \mathbf{F} vanishes. Alternatively, one can work with Majorana operators [12, 13] $a_{2n-1} = (c_n + c_n^\dagger)$ and $a_{2n} = i(c_n - c_n^\dagger)$ and form the $2N \times 2N$ correlation matrix $M_{m,n} = \langle a_m a_n \rangle$. Restricted to the subsystem, it contains the same elements as the two matrices in (18) but arranged differently. Writing $M_{m,n} = \delta_{m,n} + i\Gamma_{m,n}$, the matrix Γ of the subsystem has the eigenvalues $\pm i \tanh(\varepsilon_l/2)$.

This method is very general. It works in any dimension, for arbitrary quadratic Hamiltonians, for all states which are Slater determinants, and even at finite temperature. Thus it has been used in a large number of situations ranging from homogeneous chains to defect problems, random systems, higher dimensions and the time evolution after a quench.

Factorization properties as in (14) are well-known for Gaussians, and therefore the approach is equally applicable to coupled oscillators in the ground state (12). Thus ρ_α must be the exponential of a bosonic operator (as found in (I)) and \mathcal{H}_α is again determined such that it reproduces the correlation functions, in this case those of positions and momenta, $X_{i,j} = \langle x_i x_j \rangle$ and $P_{i,j} = \langle p_i p_j \rangle$. In analogy to (18) the single-particle eigenvalues then follow from [33, 30, 34]

$$2\mathbf{P} \, 2\mathbf{X} \, \phi_l = \coth^2\left(\frac{\varepsilon_l}{2}\right) \phi_l. \quad (19)$$

Since for the total system $2\mathcal{P} = \mathcal{V}^{1/2} = \mathcal{A}$ and $2\mathcal{X} = \mathcal{V}^{-1/2}$, the matrix on the left side of (19) is seen to be the restriction of \mathcal{A} to the subsystem multiplied by the restriction of its inverse. This is exactly the expression given in (I). As in the fermionic case, one can also combine coordinates and momenta, which are analogous to the Majorana variables, and consider the corresponding $2L \times 2L$ correlation matrix, usually called covariance matrix. Its reduction to diagonal form is a well-known problem in mathematics [35] and the resulting $\coth(\varepsilon_l/2)$ are also referred to as symplectic eigenvalues [36, 37].

The method was used for example in [38, 39, 34] and again works also at finite temperature.

(III) Via classical statistical models [40, 41]. In one dimension one can exploit the relations between quantum chains and two-dimensional classical models. The starting point is a discrete version of a path-integral representation.

Consider a quantum chain of finite length and imagine that one can obtain its state $|\Psi\rangle$ from an initial state $|\Psi_s\rangle$ by applying a proper operator T many times. If T is the row-to-row transfer matrix of a classical model, one has thereby related $|\Psi\rangle$ to the partition function of a two-dimensional semi-infinite strip of that system. The total density matrix $|\Psi\rangle\langle\Psi|$ is then given by two such strips. This is sketched on the far left of Fig.1. The reduced density matrix, e.g. for the left part of the chain, follows by identifying the variables along the right part of the horizontal edges and summing them, which means tying the two half-strips together. In this way, ρ_α is expressed as the partition function of a full strip with a perpendicular cut, as shown half left in the figure.

This procedure works for the ground state of a number of integrable quantum chains. For example, the TI chain can in this way be related to a two-dimensional Ising model on a square lattice which is rotated by 45° with respect to the horizontal [41]. In the same way, a chain of coupled oscillators is connected with a two-dimensional Gaussian model [24] and an XY chain with an Ising model on a triangular lattice [42]. Analogous correspondences link XXZ, XYZ and higher-spin chains to vertex models

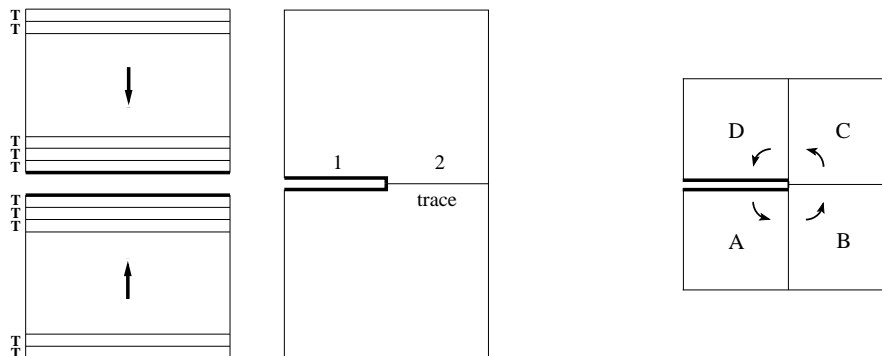


Figure 1. Left: Density matrices for a quantum chain as two-dimensional partition functions. Far left: Expression for ρ . Half left: Expression for ρ_1 . The matrices are defined by the variables along the thick lines. Right: Two-dimensional system built from four quadrants with corresponding corner transfer matrices A, B, C, D . The arrows indicate the direction of transfer. After Ref. [15].

[41, 43, 44]. To use these relations, however, one needs a way to actually calculate the resulting partition function. This is possible with the help of the corner transfer matrices (CTM's) introduced by Baxter [45]. These are partition functions of whole quadrants as shown on the right of Fig.1, or of sextants, if one is dealing with a triangular lattice. By multiplying these transfer matrices one can then obtain the reduced density matrix for a half-chain as

$$\rho_\alpha \sim ABCD. \quad (20)$$

Since ρ_α is given by an infinite strip, one also needs infinite-size CTM's in this relation. But exactly in this limit they are known for several non-critical integrable models and have the form

$$A = e^{-u\mathcal{H}_{CTM}} \quad (21)$$

where u contains the anisotropy of the two-dimensional system. This is a consequence of the star-triangle relations on which the integrability rests [46]. This approach gives \mathcal{H}_α in the original variables, see section 5.2, and explicit expressions for the single-particle eigenvalues ε_l in the diagonalized form. According to the derivation, it applies to one-half of an infinite chain, but in practice the chain has only to be much longer than the correlation length.

Summing up, we have shown how to arrive at (11) and how to obtain the ε_l . The eigenstates of ρ_α and their eigenvalues w_n then follow by specifying the occupation numbers of all single-particle levels. The analytical result for ε_l just mentioned is exceptional. For finite subsystems beyond one or two sites, one has to find the ε_l numerically. This leads to a characteristic difficulty, because the eigenvalue equations in (II) contain hyperbolic functions which approach ± 1 for large ε_l . As the subsystem size grows, more and more values lie (exponentially) close to ± 1 , and can only be obtained reliably with special techniques [47]. Therefore the values of the ε_l in most of the following figures do not exceed 20-30.

4. Spectra

In this section we give an overview of the single-particle spectra and the full ρ_α -spectra for various situations. These include different dimensions, critical and non-critical systems and the geometrical shape of the subsystem. We will focus on the ε_l because these are the primary quantities.

4.1. One dimension

(I) Non-critical chains.

For infinite TI, XY and oscillator half-chains, the CTM approach gives the universal formula

$$\varepsilon_l = \begin{cases} (2l + 1)\varepsilon & , \quad \text{disordered region} \\ 2l\varepsilon & , \quad \text{ordered region} \end{cases} \quad (22)$$

where $l = 0, 1, 2, \dots$. Thus one has *equidistant* levels and in a plot ε_l vs. l the dispersion is strictly linear. The only free parameter is the level spacing which depends on the

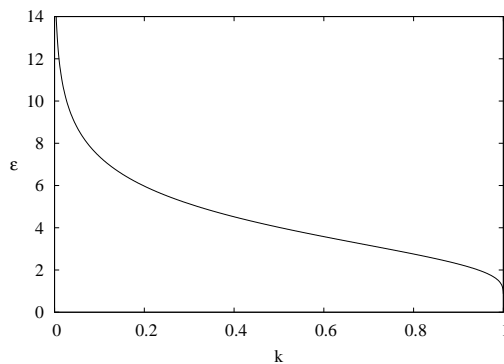


Figure 2. Level spacing as a function of the parameter k .

details of the model. It is given by

$$\varepsilon = \pi I(k')/I(k), \quad (23)$$

where $I(k)$ denotes the complete elliptic integral of the first kind, and $k' = \sqrt{1 - k^2}$. The elliptic modulus k with $0 \leq k \leq 1$ is given in the TI model by

$$k = \begin{cases} \lambda & , \quad \lambda < 1 \\ 1/\lambda & , \quad \lambda > 1 \end{cases} \quad (24)$$

In the XY model, the ordered region is subdivided by the so-called disorder line $\gamma^2 + h^2 = 1$ and one has to distinguish three cases

$$k = \begin{cases} \gamma/\sqrt{\gamma^2 + h^2 - 1} & , \quad h > 1 \\ \sqrt{\gamma^2 + h^2 - 1}/\gamma & , \quad \gamma^2 + h^2 > 1, h < 1 \\ \sqrt{(1 - \gamma^2 - h^2)/(1 - h^2)} & , \quad \gamma^2 + h^2 < 1, h < 1 \end{cases} \quad (25)$$

Here the last formula comes from a different approach [48, 49]. For the oscillator chain, k is the nearest-neighbour coupling and one has to put $\omega_0 = 1 - k$. In this case, there is no ordered region. In all models, the critical point is given by $k = 1$ and since $I(k)$ diverges for $k \rightarrow 1$, the level spacing vanishes there and the dispersion curve becomes flat. The complete behaviour of ε is shown in Fig. 2.

Results for finite TI chains are shown in Fig. 3 on the left. The linear behaviour is perfect for the smallest λ . As one comes closer to the critical point, the slope decreases as predicted, but there are also deviations from the linearity for large ε_l . Thus the linear region shrinks and is no longer visible at the critical point. This is the typical finite-size scenario in these models. On the right side, the resulting w_n , ordered by magnitude, are shown. One can see a rapid decrease with n which is fastest for the smallest λ but is still impressive at criticality (note the vertical scale). This means that a Schmidt decomposition could be truncated safely after about 10 terms and is the basis for the fantastic performance of the DMRG in this case [50].

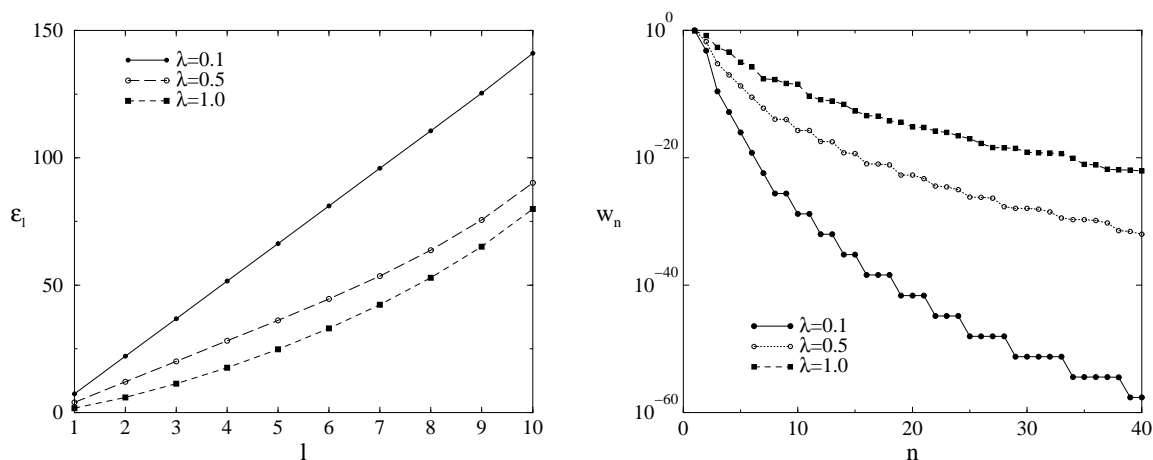


Figure 3. Density-matrix spectra for one-half of a transverse Ising chain with $N = 20$ sites in its ground state. Left: All ten single-particle eigenvalues ε_l . Right: The largest total eigenvalues w_n . Reprinted with permission from [28]. ©2001 by the APS.

The lowest w_n -curve also shows a step structure with plateaus which become longer with n . These are a consequence of the equidistant levels, a certain eigenvalue of \mathcal{H}_α can then be realized by different combinations of ε_l . The degeneracy is given by the number of partitions $P(s)$ of an integer s into other (odd or even) integers. Using asymptotic formulae for the $P(s)$, one finds the leading large- n behaviour [51]

$$w_n \sim \exp[-a(\ln n)^2] \quad (26)$$

where $a = \varepsilon 6/\pi^2$. The same result with a different constant a holds for bosons. If the dispersion is not strictly linear, the steps are smeared and a rather smooth w_n spectrum is obtained.

An important new feature appears in the ε_l -spectra, if the subsystem is a segment in a chain. Then a two-fold degeneracy is found, at least for the lowest eigenvalues. The

reason lies in the form of the eigenfunctions, which are concentrated near the ends, as will be demonstrated in section 5. This leads to a degeneracy of the w_n , with a factor of 2 for each ε_l which is involved, and therefore to a significantly slower decay.

For the spin chains, there are cases where the ground state simplifies and becomes a doublet of product states. Then one ε_l is zero, while all others diverge. As a consequence, all w_n except two collapse to zero. This happens not only in the TI model for $\lambda \rightarrow \infty$, but also in the XY model on the disorder line [28]. If the result were not known, one could locate the line from the behaviour of the spectra.

Finally, we note that also a dimerized half-filled hopping model shows such equidistant ε_l because one can relate it to the TI model via the correlation functions. The parameter k is then given by $k = (1 - \delta)/(1 + \delta)$, where $\delta > 0$ is the dimerization parameter.

(II) Critical chains.

In critical systems, the size of the subsystem affects not only the upper part of the single-particle spectrum. This is shown in Fig. 4 for a segment in a half-filled hopping model, or XX chain. The eigenvalues follow in this case from the simple correlation

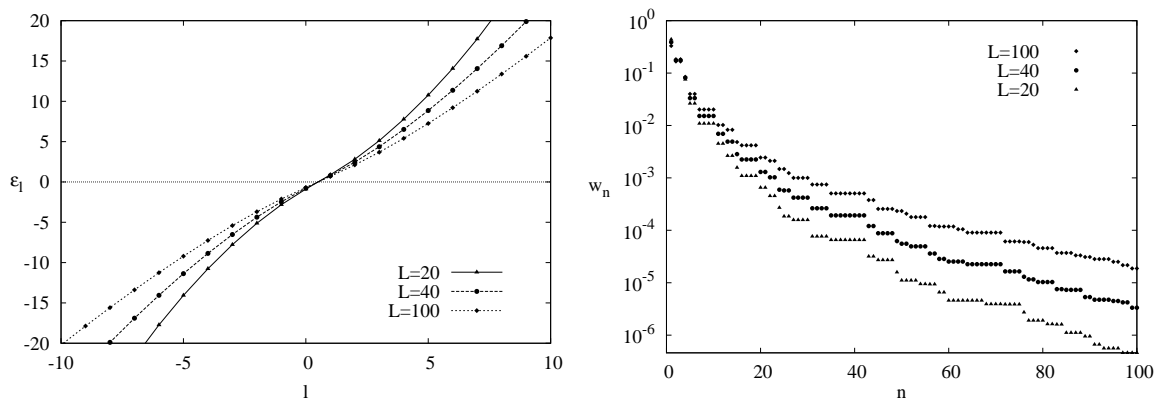


Figure 4. Size dependence of the density-matrix spectra in a critical system. Shown are results for segments of different lengths in an infinite hopping model. Left: Single-particle eigenvalues ε_l . Right: Total eigenvalues w_n . After Ref. [15].

matrix

$$C_{m,n} = \int_{-k_F}^{k_F} \frac{dq}{2\pi} e^{-iq(m-n)} = \frac{\sin(k_F(m-n))}{\pi(m-n)} \quad (27)$$

where $k_F = \pi/2$ for half filling. One sees that the whole dispersion curve is shifted towards the horizontal axis and becomes flatter as the length increases. The shift is not rapid, the first few eigenvalues vary as $1/(\ln L + b)$ with somewhat different constants b around 2.5. From a continuum approximation for the eigenvalue problem, one obtains the asymptotic formula

$$\varepsilon_l = \pm \frac{\pi^2}{2 \ln L} (2l - 1), \quad l = 1, 2, 3, \dots \quad (28)$$

which can also be derived with conformal considerations [52]. A similar expression for bosons was given in [53]. The formula is also valid for a segment of L sites at the end of a chain, if one substitutes $2 \ln L \rightarrow \ln(2L)$, which increases the values roughly by 2. It predicts the $1/\ln L$ behaviour, but also a linear dispersion as in the non-critical case. In practice, this can only be seen if in addition to L also $\ln L$ is large, which requires huge sizes. Nevertheless, it is an important guide for the understanding of the situation and will be used again later. Formulae of this type and the numerical difficulties in verifying them are known from studies of critical finite-size CTM's [54, 55, 56].

Although the change of the ε_l is slow, it has a clear effect on the w_n spectra, as seen on the right of the figure. The decay becomes significantly slower for larger systems, which means that the entanglement grows with the size. Invoking conformal results, one can obtain the functional form of the w_n -spectrum [57, 58]. Asymptotically, (26) is still valid, but now $a \sim 1/\ln L$ varies with the length. Therefore the DMRG method does not work as well in this case, although it still can handle sizes of $L \sim 100$.

Finally we want to show how certain modifications of the ground state affect the spectra. In the previous cases, the system was always half filled, which leads to a symmetric spectrum ($\pm\varepsilon_l$ appear) [29]. If the filling is varied in (27), one finds that the ε_l -dispersion curve is moved up or down in a similar way as the Fermi level, see Fig. 5. For a completely full or empty system, which is a product state (in spin language all spins are up or down), the ε_l are all infinite and w_n becomes a Kronecker symbol, $w_n = \delta_{n,1}$, as it should.

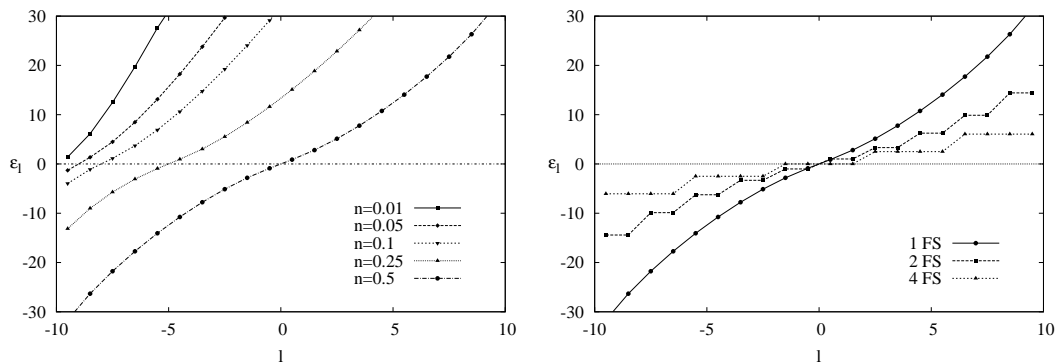


Figure 5. Single-particle spectra for different ground states. Left: Variation with the filling. Right: Variation with the number of equal-size Fermi seas at half filling. All results are for a segment of $L = 20$ sites in an infinite hopping model.

If the Fermi sea consists of several disconnected parts, one finds degeneracies in the eigenvalues, if empty and full regions in momentum space have equal size. This is shown in Fig. 5 on the right. It looks as if one had several independent kinds of particles. Effectively, the dispersion then rises only with a fraction of the slope. The same holds in the case of non-equal Fermi seas, where the degeneracies are washed out. Such a situation occurs, for example, for the ground state of the chain with an energy current [59]. As in the previous examples, the w_n then decrease more slowly and the

entanglement becomes larger.

If one modifies the hopping between the segment and the environment at one interface, one can interpolate continuously between a homogeneous chain and one with an open end. [60]. The ε_l -spectrum in this case is shown in Fig. 6 on the left. As the bond is weakened, a region with a steeper initial ascent appears before the curve follows the pattern without defect. This region can be associated with the developing free end and remains when the bond is cut completely. If, on the other hand, the bonds at both interfaces are weakened, the dispersion is shifted upwards resp. downwards as a whole and a gap develops. In the decoupling limit it goes to infinity and the entanglement vanishes.

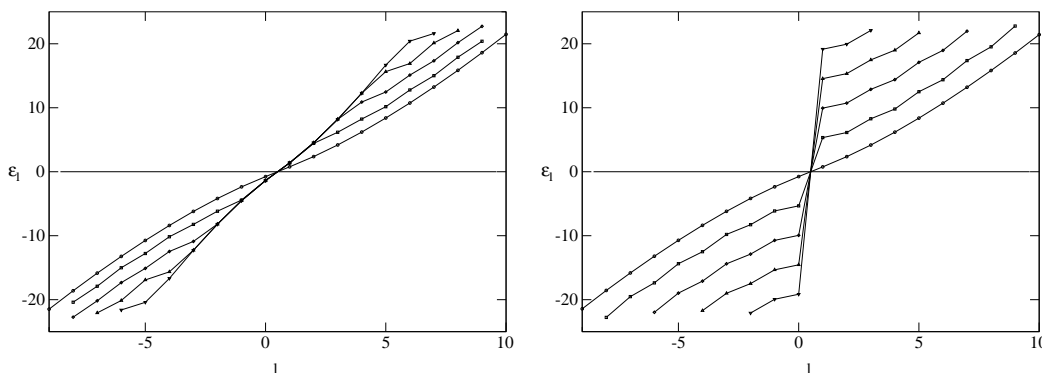


Figure 6. Influence of interface modifications on the single-particle spectra for a segment with $L = 50$ sites in a hopping model. Left: Modified bond at one end. Right: Modified bonds at both ends. The curves correspond to bond values $t = 1; 10^{-1}; 10^{-2}; 10^{-3}; 10^{-4}$, from bottom to top in the right part of the figures. After Ref. [60].

4.2. Two dimensions

(I) Non-critical systems

The simplest two-dimensional system consists of a set of M uncoupled identical parallel chains, all divided at the same point such that the subsystem has the form of a half-strip [61]. This is the usual DMRG geometry. The combined RDM is then a product of the individual ones and \mathcal{H}_α becomes a sum

$$\mathcal{H}_\alpha = \sum_{l,\mu} \varepsilon_{l,\mu} f_{l,\mu}^\dagger f_{l,\mu} \quad (29)$$

where μ is the chain index. Since $\varepsilon_{l,\mu} = \varepsilon_l$, the single-particle eigenvalues are simply M -fold degenerate. For free particles, a coupling of the chains does not change this situation because one can separate the system into M new independent chains by a Fourier transformation in the perpendicular direction [25, 62]. The index μ in (29) then becomes the Fourier index q . Only $\varepsilon_{l,q}$ will depend on q and the M -fold degenerate levels will become bands.

For coupled oscillators and an infinite half-strip, the problem can in this way be solved *exactly* by invoking the one-dimensional results. One only has to determine the elliptic parameter $k = k(q)$ for each Fourier component from the coupling k_x in the chain direction and the frequency $\omega^2(q) = \omega_0^2 + 2k_y(1 - \cos q)$ via

$$\frac{\omega(q)}{k_x} = \frac{1 - k}{k} \quad (30)$$

Numerical results for a system of 10 chains with actually finite length are shown in Fig. 7. The coupling of the chains was varied and one can see nicely, how the plateaus

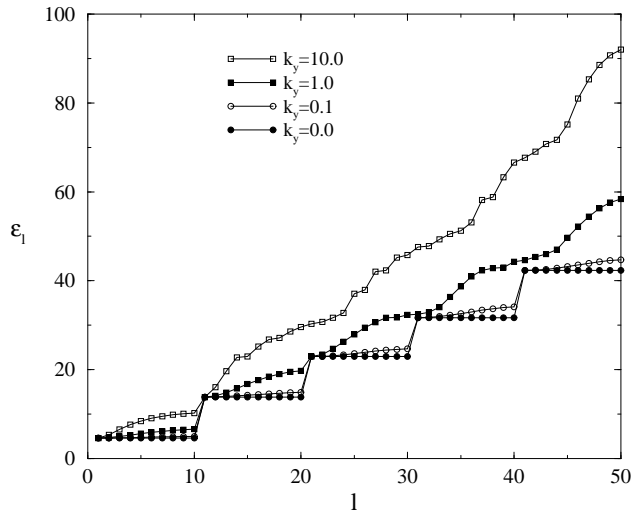


Figure 7. Single-particle eigenvalues for one-half of a 10×10 system of coupled oscillators with $\omega_0 = k_x = 1$ and different couplings k_y . Reprinted with permission from [25]. ©2000 by the APS.

with 10 levels develop into bands and a rather smooth, roughly linear curve results in the isotropic case. The initial plateaus, combined with the large freedom in the bosonic occupation numbers, lead to even larger plateaus in the w_n -spectrum. In the isotropic case, one can derive an asymptotic formula as (26) by assuming a strictly linear behaviour with a slope

$$\varepsilon_l = \lambda l = \frac{\varepsilon}{M} l \quad (31)$$

Then one finds (26) with a coefficient $a = \lambda 3/2\pi^2$. The crucial difference is that $\lambda \sim 1/M$ depends inversely on the width, which makes the decay of the w_n exceedingly slow for wide systems. The entanglement becomes correspondingly high. This is a general feature and will be taken up again in section 6. For the DMRG it means that the width of the strip puts a fundamental limit on its applicability.

For subsystems in the form of $L \times L$ squares embedded in an infinite lattice, one can obtain similar results by solving the equation (19) numerically. One finds again bands as in Fig. 7, but the number of states in the lowest bands is now given by $(4L - 4)$, which one recognizes as the the number of boundary sites. Plotting the ε_l as a function

of the scaled index $l/(4L - 4)$, the results fall essentially on top of each other. This is the same behaviour as for the single straight boundary, where l/M enters. It is a clear indication that the single-particle states are associated with the interface between the subsystem and its surrounding, as in one dimension.

(II) Critical systems

In this case one finds similar features which we will exhibit for the hopping model on a square lattice. The isotropic half-filled model has the well-known quadratic Fermi surface with corners at $(\pm\pi, 0)$ and $(0, \pm\pi)$ in momentum space. This gives the correlation function as the product of two one-dimensional ones as in (27)

$$C(x, y|0, 0) = 2 \frac{\sin(\pi(x - y)/2)}{\pi(x - y)} \frac{\sin(\pi(x + y)/2)}{\pi(x + y)} \quad (32)$$

where x and y are integers. If the model is anisotropic, the Fermi surface is more complicated and one momentum integration has to be done numerically. With these functions one can calculate the spectra for arbitrary subsystems embedded in an infinite lattice. For half filling, the spectra are again symmetric, i.e. the eigenvalues occur in pairs $\pm\varepsilon$.

Fig. 8 shows results for $L \times L$ squares, plotted to exhibit the scaling behaviour. On the left, the ε_l are shown as a function of the scaled index l/L . One can see low-lying bands which all have the same horizontal length 1 and thus contain L states. However, their height still varies with L . Only by plotting $\varepsilon_l \ln L$ they all collapse on one curve, as shown on the right. This demonstrates that, on the one hand, the linear size L enters as in the non-critical case, but that also the inverse logarithmic dependence on L found in one dimension remains. As a result, logarithmic corrections appear in the entanglement entropy, see section 6. Note also that L enters, and not $4L - 4$ as before. This is most obvious in a band of L eigenvalues which are exactly zero (the figure shows only one-half of it). The latter feature is peculiar to the square and does not occur for rectangles, where the dispersion rises smoothly from zero.

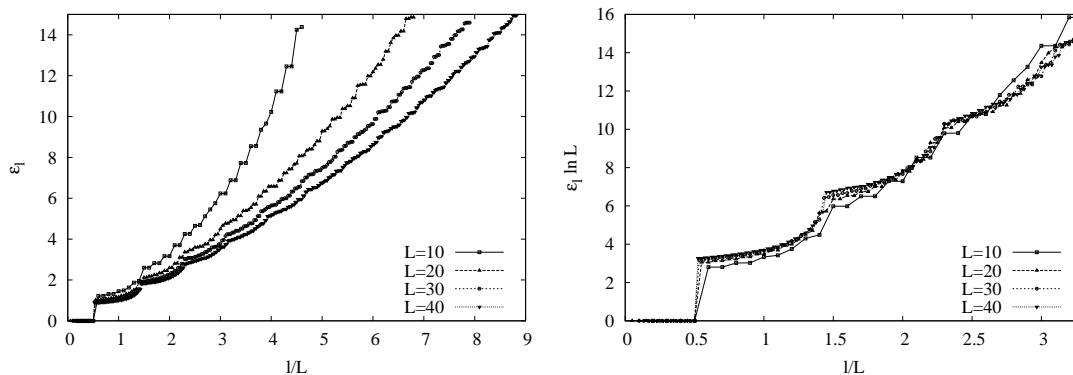


Figure 8. Single-particle spectra for $L \times L$ squares in an infinite planar hopping model. Left: ε_l vs. l/L . Right: $\varepsilon_l \ln L$ vs. l/L . Only the positive eigenvalues are shown.

The resulting spectrum of ρ_α is shown in Fig. 9 for three relatively small systems. For the 4×4 square, all 2^{16} eigenvalues are displayed and the s-shaped curve actually

reflects the symmetry of the ε_l spectrum. The 4×5 system gives much smoother results which can be fitted well by the law (26). For it, and also for the 5×5 system, the curves drop only to a value of about 10^{-4} for n around 1000, which is to be compared with the one-dimensional results of Fig. 4, where this value is reached already at $n \sim 100$ for $L = 100$. The same feature is found for other geometries [28, 47]. This shows very clearly the basic difference between one and two (and also higher) dimensions.

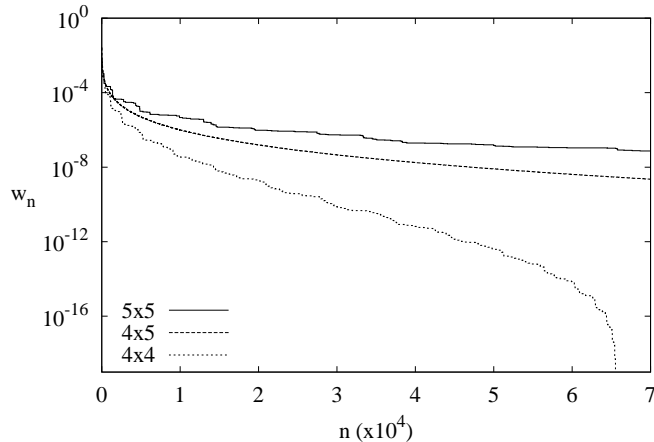


Figure 9. Total eigenvalues w_n for squares and rectangles in an infinite planar hopping model. For the 4×4 system, the figure shows *all* w_n .

5. Further aspects

5.1. Single-particle wave functions

(I) Chains

The eigenfunctions associated with the ε_l have a particular nature. In Fig.10 they are shown for the smallest ε_l in the case of a segment in a half-filled hopping model. On the left, the model is dimerized, i.e. non-critical, and one sees that the amplitude is concentrated near the two interfaces to the remainder and almost zero in the middle. This feature persists even in the homogeneous critical case seen on the right, although there is now a slow decay into the interior. For the highest ε_l , on the other hand, the amplitude is concentrated in the centre of the subsystem and the eigenfunction resembles a Gaussian. The same pattern can be seen in oscillator chains [25, 63, 36]. It is very suggestive, since it means that the states which are most important in the entanglement are those closest to the boundary. The whole entanglement appears as a phenomenon taking place within a layer whose width is given by the correlation length.

A lattice result for $\phi_l(j)$ in the hopping model is only available in the case $\varepsilon_0 = 0$ which occurs for odd L [52]. The wave function then is u-shaped and vanishes at every second site, see [64]. However, one can derive an expression in the continuum limit.

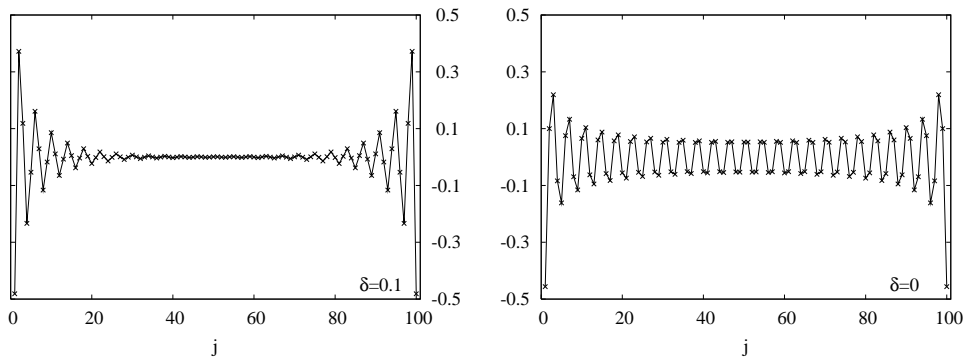


Figure 10. Lowest lying single-particle eigenstates in a dimerized ($\delta = 0.1$, left) and a homogeneous ($\delta = 0$, right) hopping model for a segment of $L = 100$ sites. After Ref. [15].

Putting $x = j/L$, it reads for a segment located between $x = 0$ and $x = 1$ [52]

$$\phi_l(x) = \frac{c}{\sqrt{x(1-x)}} \sin\left[\frac{\varepsilon_l}{2} \ln\left(\frac{x}{1-x}\right) + \alpha\right] \quad (33)$$

Such logarithmic oscillations were found earlier in CTM studies related to the TI [56] and the oscillator half-chain [65]. In the latter case, which was also treated in [53], the square-root prefactor is absent.

(II) Planar systems

It is clear that the basic feature, namely the concentration near the interface, will also be found in two dimensions. As an example, Fig. 11 shows the situation for

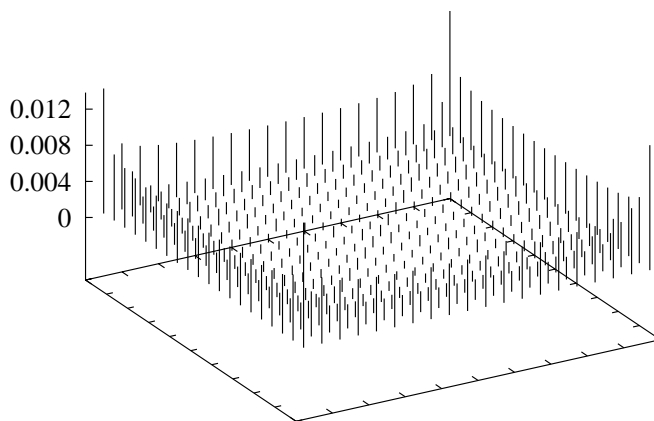


Figure 11. Squared amplitudes summed over the band of states with $\varepsilon_l = 0$ for a 20×20 square in an infinite planar hopping model.

the $\varepsilon_l = 0$ states which occur for a quadratic subsystem in a planar hopping model.

Due to the degeneracy, the individual states are not uniquely defined and one has to consider all simultaneously. The maxima at the boundary are clearly visible and one has the same u-shaped pattern as in the one-dimensional case. In addition, there is a slight enhancement along the diagonals. In general, the eigenfunctions have variations parallel to the interface which are related to the square symmetry. To bring out their “radial” behaviour one has to calculate the analogue of a radial distribution function. One then sees, apart from a small bump in the centre, a clear increase towards the boundary for all low-lying bands. This will be even more pronounced in a non-critical system.

5.2. Nature of \mathcal{H}_α

The eigenfunctions presented in the previous subsection have their origin in a particular form of the effective Hamiltonian, which we now address. In the CTM approach it is possible to give an explicit expression for \mathcal{H}_α . This is done by considering (21) in the limit of a very anisotropic system [66, 67, 68]. For the TI half-chain this leads to the result

$$\mathcal{H}_\alpha = -C \left[\sum_{n \geq 1} (2n - 1) \sigma_n^z + \lambda \sum_{n \geq 1} 2n \sigma_n^x \sigma_{n+1}^x \right] \quad (34)$$

where the constant C depends on λ . Therefore \mathcal{H}_α also describes a TI chain, but an inhomogeneous one, with coefficients which increase linearly away from the interface. In the two-dimensional problem, this reflects the wedge-shaped geometry. In the RDM context, it suppresses the influence of sites far in the interior because \mathcal{H}_α enters exponentially into ρ_α . This Hamiltonian can also be diagonalized directly [67, 68] and one recovers the result (22) for ε_l . In the limits $\lambda \rightarrow 0$ and $\lambda \rightarrow \infty$, the level structure (22) can directly be read off the coefficients in (34).

For any finite subsystem, \mathcal{H}_α can in principle be determined numerically. This is particularly simple for the homogeneous hopping model. Then the matrix elements $h_{i,j}$ follow from the correlation-matrix eigenfunctions via

$$h_{i,j} = \sum_l \phi_l(i) \varepsilon_l \phi_l(j) \quad (35)$$

The result for a segment in a chain is shown on the left of Fig. 12. The dominant elements are those for nearest-neighbour hopping and vary roughly parabolically. This is the generalization of the linear law in the semi-infinite chain to this geometry. However, there is also hopping to more distant neighbours, although with rapidly decreasing amplitude. If the segment is located at the end of a chain, one finds the same behaviour but with only one-half of the parabola, i.e. the hopping saturates at the free end. The situation for a square in a two-dimensional lattice is shown on the right of the figure. Going parallel to an edge, the hopping in this direction varies again parabolically. It is smallest close to the edge and largest halfway in between the edges. This shows that the inhomogeneity in \mathcal{H}_α always follows the same pattern. One finds it also in the XXZ model with $\Delta = 1/2$ [69].

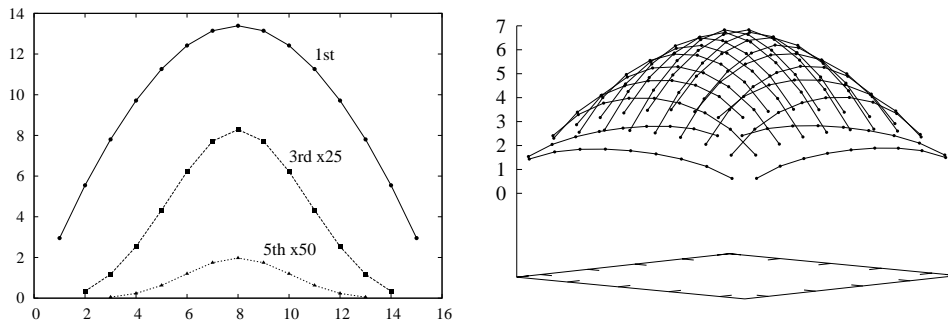


Figure 12. Matrix elements in \mathcal{H}_α for a hopping model. Left: First, third and fifth neighbour hopping in a segment of $L = 16$ sites. Right: First-neighbour hopping in a 10×10 square.

In the XX chain, one can actually show that \mathcal{H}_α for a segment commutes with the operator,

$$\mathcal{T} = \sum_{i=1}^{L-1} \frac{i(L-i)}{L} [c_i^\dagger c_{i+1} + c_{i+1}^\dagger c_i] \quad (36)$$

where the hopping is strictly only to the nearest neighbours and has *exactly* parabolic form [52]. Thus they have common eigenfunctions, and the result (33) was actually found from \mathcal{T} . Also the low-lying eigenvalues are related, and it could be that in the limit $L \rightarrow \infty$ both operators become identical up to a factor. One cannot check that numerically, however, because then large ε_l appear which are not accessible, see section 3.

5.3. Definition of a temperature

It has been pointed out in section 3 that ρ_α is not a true Boltzmann operator, since \mathcal{H}_α differs from the Hamiltonian H , as shown above. However, if the single-particle excitations have the same functional form, one can bypass this argument. This is the case for the homogeneous hopping model [70]. Then the ε_l vary linearly for large L according to (28) and the same holds for the single-particle energies in H in the vicinity of the Fermi point. For hopping to nearest neighbours with matrix element $t/2$ these are, in the subsystem, given by

$$\omega_l = t \frac{\pi}{2(L+1)} (2l-1) \quad (37)$$

Therefore, one can write $\varepsilon_l = \beta \omega_l$ with an effective temperature

$$T = t\pi \frac{\ln L}{L} \quad (38)$$

which depends on the length of the subsystem and vanishes for $L \rightarrow \infty$. Therefore ρ_α can be regarded as a true grand canonical Boltzmann distribution for all expectation values, where only the small single-particle energies are important and the wave functions do

not play a role. This holds, for example, for the particle-number fluctuations in the subsystem, which vary as TL at finite temperatures. Inserting (38), this is turned into the $\ln L$ -behaviour for the segment in the chain.

5.4. Thermal states

Although our interest is in ground-state properties, it is instructive to see what happens if one calculates ρ_α for a system at a finite temperature. This is quite easy with the correlation function approach, and the resulting spectra for the homogeneous half-filled hopping model with $t = 1$ are shown in Fig. 13. The steepest curve is the ground-state

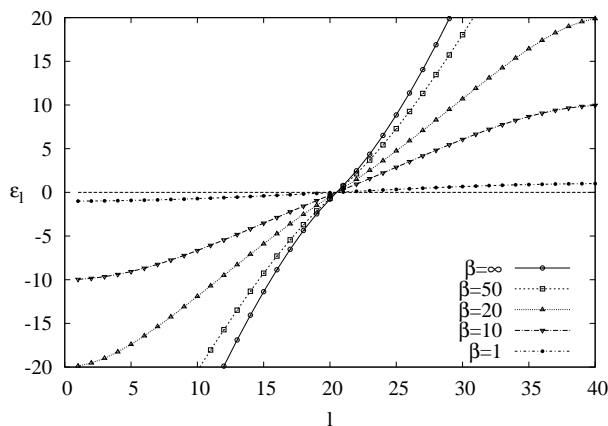


Figure 13. Single-particle spectrum as a function of the inverse temperature for a segment of $L = 40$ sites in an infinite hopping model.

result. As the temperature is increased it flattens, bends over and assumes the shape of the dispersion $\omega_q = -\cos q$ for the single-particle energies in H . In fact, one can write, expanding the Fermi function for $\beta = 1/k_B T \ll 1$

$$\begin{aligned} C_{m,n} &= \int_{-\pi}^{\pi} \frac{dq}{2\pi} e^{-iq(m-n)} f(\omega_q) \simeq \int_{-\pi}^{\pi} \frac{dq}{2\pi} e^{-iq(m-n)} \frac{1}{2} \left(1 + \beta \frac{\cos q}{2}\right) \\ &= \frac{1}{2} \left[\delta_{m,n} + \frac{\beta}{4} (\delta_{m,n+1} + \delta_{m,n-1}) \right] \end{aligned} \quad (39)$$

which has eigenvalues in the subsystem

$$\zeta_l = \frac{1}{2} \left(1 + \beta \frac{\cos q_l}{2}\right), \quad q_l = \frac{\pi}{L+1} l, \quad l = 1, 2, \dots, L \quad (40)$$

and gives

$$\varepsilon_l = -\beta \cos q_l \quad (41)$$

In other words, for high temperature

$$\mathcal{H}_\alpha \rightarrow \beta H_\alpha \quad (42)$$

which is a very plausible result. Apart from the shape of the spectrum, the essential point is that the level spacing is reduced from a value of order one to $\sim 1/L$. Such a situation is also found in quenches, see section 7.

6. Entanglement entropy

In this section, we show how the properties of the RDM spectra seen in section 4 translate into the behaviour of the entanglement entropy. Due to the form of the ρ_α it is given by the same expression as in statistical physics

$$S = \pm \sum_l \ln(1 \pm e^{-\varepsilon_l}) + \sum_l \frac{\varepsilon_l}{e^{\varepsilon_l} \pm 1} \quad (43)$$

where the upper(lower) sign refers to fermions(bosons). From this formula, one can immediately draw two general conclusions

- The largest contributions come from small ε_l (corresponding to high temperature in usual thermodynamics). Therefore the entropy will be particularly large in critical systems. For fermions its maximum value of $L \ln 2$ is reached if all ε_l vanish.
- If all ε_l are m -fold degenerate, the value of S is m times its value without degeneracy. This answers e.g. how S compares for one or two (noncritical) interfaces, or for one or two Fermi seas.

(I) One dimension

Analytical results can be given for the non-critical half-chains with the spectrum (22). The sums then lead to elliptic integrals [60] and one obtains for fermions in the disordered region

$$S = \frac{1}{24} \left[\ln \left(\frac{16}{k^2 k'^2} \right) + (k^2 - k'^2) \frac{4I(k)I(k')}{\pi} \right], \quad (44)$$

while for bosons the formula is

$$S = -\frac{1}{24} \left[\ln \left(\frac{16k'^4}{k^2} \right) - (1 + k^2) \frac{4I(k)I(k')}{\pi} \right]. \quad (45)$$

A similar expression with an additional contribution of $\ln 2$ coming from the eigenvalue $\varepsilon_0 = 0$ holds in the ordered region. Also the results for XXZ and XYZ chains [72, 43] can be brought in this form. The entropy for the anisotropic XY chain with $h = 0$ can be written as the sum of the expressions in the ordered and the disordered region [42, 71]. A plot of S , based on a numerical evaluation of the sums, was first shown in [72]. Curves for the XY model can be found in [73]. The case of a segment in an XY chain was treated even before the half-chain. Using the correlation matrix and solving a Riemann-Hilbert problem, S was obtained as an integral over theta functions [48, 49]. This is equivalent to the half-chain result multiplied by two.

In the disordered region there is little difference between fermions and bosons. The values of S are typically of order one or smaller, so that the corresponding ground states have $M_{\text{eff}} \sim 1 - 10$ states in the Schmidt decomposition. This reflects the rapid decay of the spectrum in Fig. 3. An exception is only the vicinity of the critical point. As anticipated, S becomes large there and actually diverges for this geometry. The formulae give for $k \rightarrow 1$

$$S \simeq \frac{c}{6} \ln \left(\frac{1}{1-k} \right) \quad (46)$$

where $c = 1/2$ for the TI model and $c = 1$ for the bosons. Since the correlation length varies as $\xi \sim 1/(1 - k)$, the logarithm is of the form $\ln(\xi/a)$ [72].

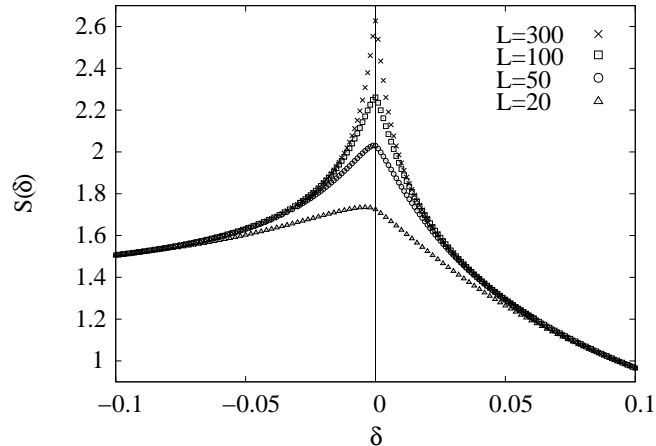


Figure 14. Entanglement entropy for segments of different size L in a one-dimensional hopping model as a function of the dimerization parameter δ . The development of a singularity in case of vanishing dimerization is clearly visible. After Ref. [15].

The behaviour for a finite subsystem is shown in Fig. 14 for segments in a dimerized hopping model. In this case, S no longer diverges at criticality but shows a maximum which becomes higher with increasing L . The size dependence at the critical point can be obtained in a very simple way [53]. Using the asymptotic form (28) of the ε_l in (43) and converting the sums into integrals gives

$$S = \frac{2 \ln L}{\pi^2} \left[\int_0^\infty d\varepsilon \ln(1 + \exp(-\varepsilon)) + \int_0^\infty d\varepsilon \frac{\varepsilon}{\exp(\varepsilon) + 1} \right] \quad (47)$$

and since both integrals equal $\pi^2/12$ one finds

$$S = \frac{1}{3} \ln L \quad (48)$$

On the lattice, this behaviour was first found numerically [12, 13] and then by using the asymptotic properties of the correlation matrices [74, 75]. The general formula for critical chains is

$$S = \nu \frac{c}{6} \ln L + k \quad (49)$$

Here c is the central charge, ν the number of contact points between the (singly-connected) subsystem and the remainder of the chain, and k a non-universal constant which depends on the model parameters and the geometry. An estimate for k can be obtained if one replaces $\ln L \rightarrow \ln L + 2.5$ in (47), using the scaling found for the first few eigenvalues. This gives $k \sim 0.8$ for the hopping model, whereas the correct value is $k = 0.726$. As the numerics show, the logarithmic behaviour of S can already be observed in relatively small systems, where (28) is not yet valid. Since it holds for all conformally invariant models [7, 72] the formula (49) is a central result.

The interpolation between one and two contact points via a modified bond has already been discussed in section 4.1. Regarding the entropy, it can be described by an effective central charge $c_{\text{eff}} = \nu c/2$ in (49) which varies continuously between 1/2 and 1. The spectrum on the left of Fig. 6 then leads to the result in Fig. 15. A formula

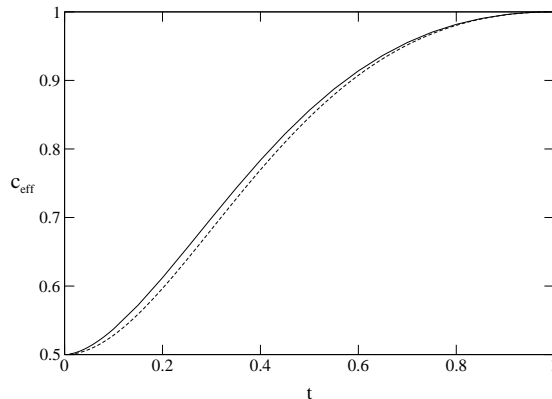


Figure 15. Effective central charge for one interface defect in a hopping model as a function of the defect strength. The dotted curve is an analytical approximation. After Ref. [60].

for c_{eff} based on boundary conformal theory was given in [76]. The problem was also generalized to the case of two coupled planes [77]. Completely inhomogeneous systems were studied in the form of chains with extended defects [78], gradients [79], aperiodic [80] and random [81, 82, 83] couplings. On the other hand, one can consider situations where the subsystem is not singly connected and thus has many contact points. For comb-like geometries, the leading term in S then becomes proportional to L [84]. For example, if the sites of the subsystem are two lattice spacings apart, one has $S = L \ln 2$ in the hopping model. This is a direct consequence of (27) which reduces to $C_{i,j} = \delta_{i,j}/2$ and gives $\varepsilon_l = 0$ for all l . Conformal results for multiple intervals are reviewed in [58].

(II) Two dimensions

The influence of the interface on the spectra in two dimensions has already been demonstrated in section 4.2. In the entanglement entropy, it leads to the famous “area law” which has been the topic of many investigations, see [85] for a recent review. Consider, for example, the non-critical half-strip of oscillators. Each band of $\varepsilon_{l,q}$ contributes an amount of order M to S which thereby becomes proportional to the length of the interface. Expressed differently, S is the sum of the M individual q -chain entropies and can be written, for large M ,

$$S = \sum_{l,q} s_{l,q} \simeq M \int_0^\pi \frac{dq}{\pi} \sum_l s_{l,q} \quad (50)$$

For a square-shaped subsystem where the lowest band contains as many states as there are interface sites, one obtains an analogous result.

The argument also holds for critical systems [62]. Regarding a two-dimensional hopping model as a system of coupled chains, the Hamiltonian reads, for $t = 1$,

$$H = - \sum_q \sum_n \left[\frac{1}{2} (c_{n,q}^\dagger c_{n+1,q} + c_{n+1,q}^\dagger c_{n,q}) + \cos q c_{n,q}^\dagger c_{n,q} \right] \quad (51)$$

Thus for each q -value one has a chain with a chemical potential $\mu = \cos q$. This affects the filling but does not change the $\ln L$ -behaviour of S , which therefore becomes proportional to $M \ln L$. This is still an area law, but the occurrence of the second length disturbs the picture somewhat. The same holds for a square $L \times L$ subsystem with the spectrum found in Fig. 8. There the number of states scales as L but the value of the ε_l as $1/\ln L$. Thus one finds logarithmic corrections to the area law. This was proven exactly by constructing bounds on S [86, 87, 88] and an expression for the prefactor was given in [87]. The problem was also investigated numerically in two [39, 89] and three [89] dimensions, and the presence of the logarithm traced to a finite Fermi surface in the system. For bosonic systems, on the other hand, no logarithmic corrections were found in the critical limit.

Finally, we want to comment briefly on the largest eigenvalue w_1 of the RDM, which has a close relation to S . It plays a role in the so-called single-copy entanglement, where one asks which maximally entangled state one can reach from an initial state [90]. From (11) one sees that

$$w_1 = \frac{1}{Z} e^{-E_0} \quad (52)$$

where E_0 is the smallest eigenvalue of \mathcal{H}_α . This can be evaluated for the non-critical half-chains in the same way as S . For example, putting $S_1 = -\ln w_1$, one finds in the bosonic case

$$S_1 = -\frac{1}{24} \left[\ln \left(\frac{16k'^4}{k^2} \right) - \pi \frac{I(k')}{I(k)} \right]. \quad (53)$$

In the critical limit, this diverges as S and one finds that $S_1 \rightarrow S/2$. The same holds for fermions [90, 91]. One can show that this is a general result for conformally invariant systems [91, 92, 93].

7. Entanglement evolution

In this last chapter we present results on the entanglement evolution after a change of the Hamiltonian $H_0 \rightarrow H_1$. This can be treated via correlation functions as before and leads to interesting phenomena. The simplest case is a quench, where the change is instantaneous and generates a unitary time evolution $|\psi(t)\rangle = e^{-iH_1 t} |\psi_0\rangle$. If H_1 is also a free-particle operator, the arguments work as before [94] and the RDM has the exponential form (11) as in equilibrium but with a time dependent operator

$$\mathcal{H}_\alpha(t) = \sum_{l=1}^L \varepsilon_l(t) f_l^\dagger(t) f_l(t). \quad (54)$$

In the case of particle conservation, the eigenvalues $\varepsilon_l(t)$ follow again from the restricted correlation matrix, but now taken at time t

$$C_{i,j}(t) = \langle \psi_0 | c_i^\dagger(t) c_j(t) | \psi_0 \rangle. \quad (55)$$

Therefore, one only needs to determine the time evolution of the operators $c_j(t)$ in the Heisenberg picture. In the following we discuss three different situations.

7.1. Global quench

In a global quench, the system is modified everywhere in the same way, a situation which can actually be realized in optical lattices [95]. Then the initial state becomes a highly excited state of H_1 with an extensive excess energy.

An example which illustrates the situation very well is a hopping model which is initially fully dimerized ($\delta = 1$) and then made homogeneous ($\delta = 0$). The time evolution of the correlation matrix is then given explicitly in terms of Bessel functions [96]

$$C_{m,n}(t) = \frac{1}{2} \left[\delta_{m,n} + \frac{1}{2}(\delta_{n,m+1} + \delta_{n,m-1}) + e^{-i\frac{\pi}{2}(m+n)} \frac{i(m-n)}{2t} J_{m-n}(2t) \right] \quad (56)$$

The resulting single-particle spectra are shown on the left of Fig. 16. One sees that the dispersion is linear near zero and that its slope decreases with time. This leads to the initial increase of the entropy shown on the right of the figure. For times $t \gg L/2$, however, the ε_l approach a limiting curve and S saturates. The asymptotic form of the spectrum can be obtained from the tridiagonal correlation matrix $C_{m,n}(\infty)$ as in section 5.4

$$\zeta_l(\infty) = \frac{1}{2}(1 + \cos q_l), \quad q_l = \frac{\pi}{L+1}l, \quad l = 1, 2, \dots, L \quad (57)$$

leading to

$$\varepsilon_l(\infty) = 2 \ln \tan(q_l/2). \quad (58)$$

The spacing of the q_l is proportional to $1/L$ and gives an extensive entropy $S = L(2 \ln 2 - 1)$, a value which was also found in [94] for a similar quench in the TI model. An initial state where the sites are alternatingly full and empty, would even give the maximal possible value $S = L \ln 2$.

The build-up of an extensive entropy is a typical signature of global quenches. It was given a phenomenological description in terms of emitted pairs of quasiparticles which create entanglement between the subsystem and the remainder of the system [94, 58]. In our case these quasiparticles have maximum velocity $v = 1$. This simple picture also accounts for the “light-cone effect” [97, 98] reflected in the entropy at $t \approx L/2$, where the linear increase turns into a saturation. If one starts from an inhomogeneous state the increase of S can also be non-linear [79]. A closed expression for $S(t)$ in the XY model was given in [99].

From the extensivity of S one might conjecture a relation of the quench state to a true thermal state. But a comparison of the spectra in Figs. 13 and 16 shows that,

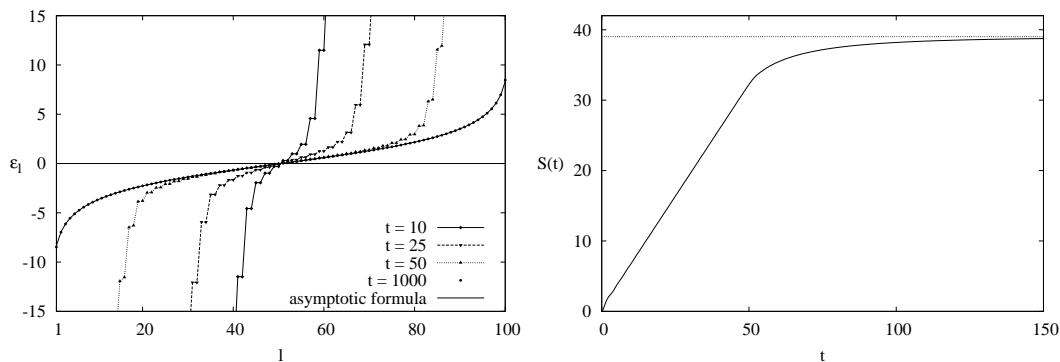


Figure 16. Global quench in a hopping model, starting with a fully dimerized initial state. Left: Time evolution of the single-particle spectrum for a segment of $L = 100$ sites. After [96]. Right: Entanglement entropy with the asymptotic value.

apart from the linear region, they are different. A calculation of $\mathcal{H}_\alpha(\infty)$ via (35) shows that it has long-range hopping which decreases as $1/|i - j|$ in the interior. However, there *are* cases, where the final effective Hamiltonian resembles H . This happens e.g. if one starts from a chain with alternating site energies $\pm\Delta$. Then one finds that for large Δ the asymptotic ε_l have the form (41) with $\beta = 2/\Delta$. This explains the observations in [100]. In general, the emergence of a $\rho_\alpha(\infty)$ after a global quench may still be viewed as a local thermalization and is a rather general feature of one-dimensional integrable systems, see e.g. [101, 102] for a rigorous treatment.

7.2. Local quench

A very different behaviour is obtained if one makes sudden local changes in the system, for example by removing defects in a hopping model. The resulting entanglement evolution has been investigated for various situations and geometries [96, 103, 104, 58]. We will consider here the case where a finite segment is joined to an infinite half-chain either on one or on both sides [104]. These two setups will be called the semi-infinite and the infinite geometry, respectively.

The time evolution of the Fermi operators $c_n(t)$ is again given in terms of Bessel functions, and in the infinite geometry the correlation matrix reads

$$C_{m,n}(t) = i^{n-m} \sum_{j,l} i^{j-l} J_{m-j}(t) J_{n-l}(t) C_{j,l}(0). \quad (59)$$

The double sum over all sites j, l has in this case to be evaluated numerically. In the semi-infinite geometry, a similar expression is obtained.

On the left of Fig. 17 we show the low-lying single-particle spectrum for the semi-infinite case on a logarithmic time scale. Since the segment is initially unentangled, all $\varepsilon_l(0) = \infty$ first drop and evolve to a transient regime up to $t \approx 2L$ where all but one relax to the stationary eigenvalues of the equilibrium chain. The remaining *anomalous* eigenvalue evolves rather slowly showing avoided crossings with the already relaxed

levels. The large-time behaviour is therefore characterized by a slow approach to the local equilibrium state.

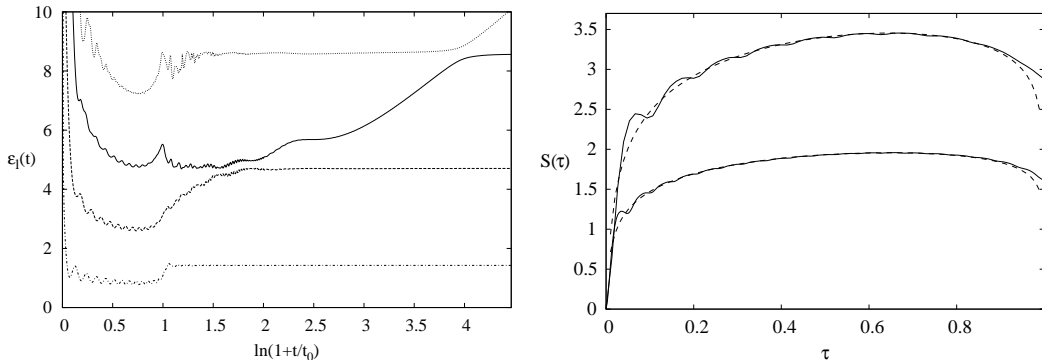


Figure 17. Left: Time evolution of the lowest $\varepsilon_l(t)$ for $L = 40$. The parameter t_0 is chosen such that $t = 2L$ gives 1 on the horizontal axis. Right: Entropy evolution in the rescaled plateau region for $L = 60$. Upper curve: Infinite geometry, lower curve: Semi-infinite geometry. After [104].

The resulting entropy evolution in the transient region is shown on the right of Fig. 17. For both geometries one can see a plateau with a characteristic shape but the height and the length are different. The latter effect is already scaled out in the figure by choosing $\tau = t/L$ for the infinite and $\tau = t/2L$ for the semi-infinite case. Using methods of conformal field theory [103, 104], one can derive analytical formulae for both cases

$$S(t) = \nu \frac{c}{6} \ln \left[\frac{4L}{\nu\pi} t \sin \left(\frac{\nu\pi t}{2L} \right) \right] + k_\nu \quad (60)$$

where ν is the number of contact points and k_ν is a constant which depends on the geometry. These curves are indicated by the dashed lines in the figure and, apart from deviations at the ends of the interval, are in good agreement with the numerical data. For $t \ll L$, Eq. (60) gives a *logarithmic* entropy growth in contrast to the *linear* increase in case of the global quench. If $L \rightarrow \infty$ this behaviour persists for all times.

The emergence of the plateau region can be related to a front starting from the defect site and propagating with unit velocity. It becomes clearly visible if one looks at the eigenvectors belonging to the $\varepsilon_l(t)$ in Fig. 17. The plateau ends when the front leaves the subsystem, which also explains the doubling of the length due to reflection in the semi-infinite case. In addition to these traveling fronts, which represent the maximal-velocity excitations, there are also more subtle signatures of the slowest ones. These are visible as flat parts in the evolution of the anomalous eigenvalue.

In the above examples we have considered defects which initially cut the system into separate pieces. However, the behaviour is rather similar, if initially the corresponding bonds are only weakened. Only the height of the plateau decreases. Since $S(t)$ is proportional to c in Eq. (60), this decrease can be described by effective central charges [96]. These depend smoothly on the initial defect strength and one obtains similar curves as in the equilibrium situation depicted in Fig. 15. A plateau is also found for local

quenches in a non-critical TI chain. The difference in this case is that it becomes flat and does not scale with the subsystem length [104]. In summary, for a finite subsystem a local quench is characterized by bursts of the entanglement: a rapid development of a plateau region is followed by a slow relaxation towards a local equilibrium.

7.3. Periodic quench

As a final example, we discuss a periodic sequence of changes $H_0 \leftrightarrow H_1$ and its effect on the entanglement. The change in the Hamiltonian can be either global or local.

In the global case, we consider again the dimerized hopping model and switch periodically between dimerizations $\pm\delta$ [105, 106]. This corresponds to a simple interchange of weak and strong bonds. The time-evolution operator up to the end of the n -th period reads

$$U(2n\tau) = U^n \quad , \quad U = U_0 U_1 = e^{-iH_0\tau} e^{-iH_1\tau} \quad (61)$$

where τ is the length of a half-period. For arbitrary times between periods n and $n+1$ one has to multiply $U(2n\tau)$ by an additional unitary operator. Thus, the problem reduces to finding the diagonal form of U which can be done analytically by a Fourier transformation. It is convenient to write it as a single exponential of an average Hamilton operator

$$U = e^{-i\bar{H}2\tau} \quad , \quad \bar{H} = \sum_q \nu_q (\xi_q^\dagger \xi_q - \eta_q^\dagger \eta_q) \quad (62)$$

with Fermi operators ξ_q and η_q . In the case $\delta = 1$, the single-particle energies are given by $\nu_q = \gamma_q/2\tau$ where

$$\cos \gamma_q = \cos^2 \tau - \sin^2 \tau \cos q \quad (63)$$

The time evolution of the entropy is obtained again from (55) and depicted on the left of Fig. 18 for several values of the dimerization δ and fixed $\tau = 0.4\pi$. The overall behaviour is an initial, step-like increase followed by a sharp bend and a final approach to an asymptotic value. The steps are sharp in the fully dimerized case, but for smaller δ they become washed out and their height ΔS decreases. For general δ and τ the entropy displays additional slow oscillations.

The characteristics of the time evolution can be understood from the dispersion of ν_q . For $\delta = 1$ and $\tau = \pi/2$ it is strictly linear, resulting in a completely regular staircase with $\Delta S = 4 \ln 2$. Thereby a segment of size L becomes maximally entangled after $L/4$ periods. This case also gives an *exact* lattice example of the quasiparticle picture in [94]. In the general case, ν_q becomes more complicated and can have several local maxima, which give rise to the slow oscillations in S .

Apart from the fine structure, the picture is similar to that of the single quench. Both problems become identical in the limit of very rapid switching, $\tau \rightarrow 0$. Then the average Hamiltonian is just the simple average $\bar{H} = (H_0 + H_1)/2 = H$ and one recovers the quench to the homogeneous chain. However, the asymptotic entropy seems

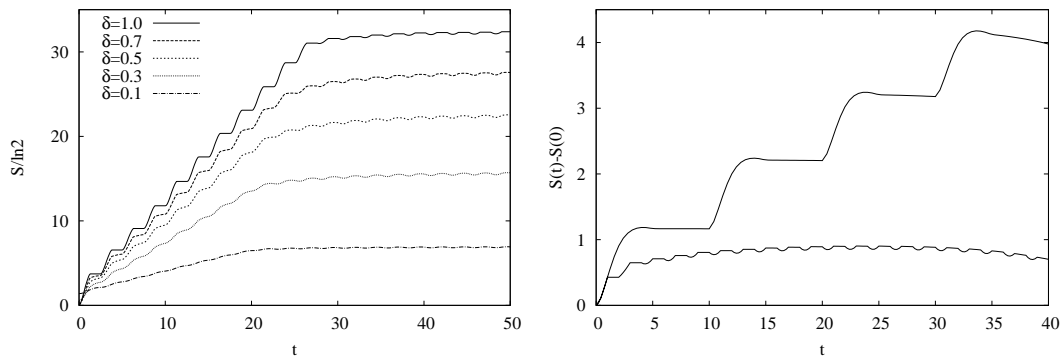


Figure 18. Entropy evolution in periodic quenches for $L = 40$. Left: Periodically switched dimerization for $\tau = 0.4\pi$ and various δ . After [105]. Right: Periodically connected chains. Upper curve: $\tau = 5$, lower curve: $\tau = 1$.

to be always larger in the periodic case, and in general is a complicated non-monotonic function of τ [105].

On the right of Fig. 18 we show results for a local periodic quench. Here two halves of an infinite hopping model are periodically connected and separated. The subsystem consists of the first L sites in one of the initially disconnected chains. One sees a characteristic difference. For a large half-period τ , one has a step structure like in the case of the global quench, and the entropy grows linearly with the number of the periods. This is the result found analytically in [107] by studying a continuum model and taking the subsystem as one of the half-chains. For small τ , however, the entropy curve resembles the plateau of a single local quench, with an additional fine structure due to the switching. In this case, the entropy grows only logarithmically. The interpretation is that, for slow switching, the system has enough time to recover and thereby the entanglement gain repeats itself after each new connection. For rapid switching, this is not the case, and for $\tau \rightarrow 0$ one recovers a single quench as before. The transition between both regimes occurs around $\tau = \pi/2$. The phenomenon can also be seen in interacting systems [108].

8. Conclusion

We have shown that the reduced density matrices of free lattice models have a special structure. This permits to view entanglement questions in these systems as thermodynamic problems and provides a very clear physical picture of the situation. In particular, the entanglement entropy can be understood from the character and the scaling behaviour of the single-particle spectra, as for conventional thermodynamical systems. Therefore the emphasis throughout the review was on the properties of these spectra. In addition to presenting them for a number of important situations, we also discussed the character of the corresponding eigenfunctions and of the effective Hamiltonian itself. Thereby the role of the interface between the two parts of the system entered in a natural way. From the character of the eigenfunctions in the ground

state problem, one can say that the entanglement “resides” mainly near the interface [12]. Therefore the states are rather weakly entangled in one dimension, but already in two dimensions this is no longer true and limits the applicability of the DMRG seriously. On the other hand, this role of the interface is not a general feature. Not only at finite temperatures, but also after global quenches, the entanglement entropy becomes extensive and typically the whole bulk of the subsystem is involved in the entanglement. On the other hand, simple local quenches only lead to logarithmic effects and time-dependent DMRG can be done. We have only considered quenches, but there are also results for continuous changes, see e.g. [109, 110], which one could discuss in the same way as here. On the whole, time-dependent phenomena should be the area of further applications. Of course, the study of non-interacting systems is always combined with the hope that they serve as guides for more realistic ones. For the DMRG this is certainly the case.

Acknowledgments

We would like to thank Pasquale Calabrese for a critical reading of the manuscript. VE is grateful to the Freie Universität Berlin for hospitality during his visit where part of this work was carried out. He acknowledges financial support by the Danish Research Council and QUANTOP.

References

- [1] Dirac P A M 1930 *Proc. Cambr. Phil. Soc.* **26** 376
- [2] Fock V 1931 *Z. Physik* **61** 126
- [3] Watanabe S 1939 *Z. Physik* **113** 482
- [4] Schrödinger E 1935 *Naturwissenschaften* **23** 807
- [5] Bombelli L, Koul R K, Lee J and Sorkin R D 1986 *Phys. Rev. D* **34** 373
- [6] Srednicki M 1993 *Phys. Rev. Lett.* **71** 666
- [7] Holzhey C, Larsen F and Wilczek F 1994 *Nucl. Phys. B* **424** 443
- [8] White S R 1992 *Phys. Rev. Lett.* **69** 2863
- [9] White S R 1993 *Phys. Rev. B* **48** 10345
- [10] Peschel I, Wang X, Kaulke M and Hallberg K, eds 1999 *Density-Matrix Renormalization* vol 528 of *Lecture Notes in Physics* (Berlin: Springer)
- [11] Schollwöck U 2005 *Rev. Mod. Phys.* **77** 259
- [12] Vidal G, Latorre J I, Rico E and Kitaev A 2003 *Phys. Rev. Lett.* **90** 227902
- [13] Latorre J I, Rico E and Vidal G 2004 *Quantum Inf. Comput.* **4** 48
- [14] Amico L, Fazio R, Osterloh A and Vedral V 2008 *Rev. Mod. Phys.* **80** 517
- [15] Peschel I and Eisler V in *Computational Many-Particle Physics* Fehske H, Schneider R and Weisse A, eds 2008 *Lecture Notes in Physics* vol 739 (Berlin: Springer) pp 581-596
- [16] Ekert A and Knight P L 1995 *Am. J. Phys.* **63** 415
- [17] Horn R and Johnson C 1991 *Topics in Matrix Analysis* (Cambridge University Press) chap 3
- [18] Schmidt E 1907 *Math. Annalen* **63** 433
- [19] Li H and Haldane F D M 2008 *Phys. Rev. Lett.* **101** 010504
- [20] Löwdin P-O 1955 *Phys. Rev.* **97** 1474
- [21] Plenio M B and Virmani S 2007 *Quantum Inf. Comput.* **7** 1
- [22] Sato J, Shiroishi M and Takahashi M 2006 *J. Stat. Mech.* P12017

- [23] Sato J and Shiroishi M 2007 *J. Phys. A: Math. Theor.* **40** 8739
- [24] Peschel I and Chung M-C 1999 *J. Phys. A: Math. Gen.* **32** 8419
- [25] Chung M-C and Peschel I 2000 *Phys. Rev. B* **62** 4191
- [26] Han D, Kim Y S and Noz M E 1999 *Am. J. Phys.* **67** 61
- [27] Braunstein S L and van Loock P 2005 *Rev. Mod. Phys.* **77** 513
- [28] Chung M-C and Peschel I 2001 *Phys. Rev. B* **64** 064412
- [29] Cheong S A and Henley C L 2004 *Phys. Rev. B* **69** 075111
- [30] Peschel I 2003 *J. Phys. A: Math. Gen.* **36** L205
- [31] Latorre J I and Riera A 2009 in this special issue
- [32] Lieb E, Schultz T and Mattis D 1961 *Ann. Phys.* **16** 407
- [33] Audenaert K, Eisert J, Plenio M B and Werner R F 2002 *Phys. Rev. A* **66** 042327
- [34] Cramer M, Eisert J, Plenio M B and Dreißig J 2006 *Phys. Rev. A* **73** 012309
- [35] Williamson J 1936 *Am. J. Math.* **58** 141
- [36] Botero A and Reznik B 2004 *Phys. Rev. A* **70** 052329
- [37] Adesso G and Illuminati F 2007 *J. Phys. A: Math. Theor.* **40** 7821
- [38] Casini H and Huerta M 2005 *J. Stat. Mech.* P12012
- [39] Barthel T, Chung M-C and Schollwöck U 2006 *Phys. Rev. A* **74** 022329
- [40] Nishino T and Okunishi K 1997 *J. Phys. Soc. Jpn.* **66** 3040
- [41] Peschel I, Kaulke M and Legeza Ö 1999 *Ann. Physik (Leipzig)* **8** 153
- [42] Peschel I 2004 *J. Stat. Mech.* P12005
- [43] Ercolessi E, Evangelisti S and Ravanini F 2009 e-print arXiv:0905.4000
- [44] Weston R 2006 *J. Stat. Mech.* L03002
- [45] Baxter R J 1982 *Exactly Solved Models in Statistical Mechanics* (London: Academic Press)
- [46] for a brief overview see: Cardy J L in *Fields, Strings and Critical Phenomena* Brezin E and Zinn-Justin J, eds 1990 *Les Houches Summer School Session* vol 49 p 169
- [47] Chung M-C 2002 Ph.D. thesis Freie Universität Berlin unpublished
- [48] Its A R, Jin B-Q and Korepin V E 2005 *J. Phys. A: Math. Gen.* **38** 2975
- [49] Its A R and Korepin V E 2009 in this special issue
- [50] Legeza Ö and Fáth G 1996 *Phys. Rev. B* **53** 14349
- [51] Okunishi K, Heida Y and Akutsu Y 1999 *Phys. Rev. E* **59** R6227
- [52] Peschel I 2004 *J. Stat. Mech.* P06004
- [53] Callan C and Wilczek F 1994 *Phys. Lett. B* **333** 55
- [54] Truong T T and Peschel I 1988 *J. Phys. A: Math. Gen.* **21** L1029
- [55] Davies B 1989 *Physica A* **159** 171
- [56] Davies B and Pearce P A 1990 *J. Phys. A: Math. Gen.* **23** 1295
- [57] Calabrese P and Lefevre A 2008 *Phys. Rev. A* **78** 032329
- [58] Calabrese P and Cardy J L 2009 in this special issue
- [59] Eisler V and Zimborás Z 2005 *Phys. Rev. A* **71** 042318
- [60] Peschel I 2005 *J. Phys. A: Math. Gen.* **38** 4327
- [61] du Croo de Jongh M S L 1999 Ph.D. thesis Leiden University unpublished
- [62] Cramer M, Eisert J and Plenio M B 2007 *Phys. Rev. Lett.* **98** 220603
- [63] Gaite J 2001 *Mod. Phys. Lett. A* **16** 1109
- [64] Cheong S A and Henley C L 2004 *Phys. Rev. B* **69** 075112
- [65] Peschel I and Truong T T 1991 *Ann. Phys.* **48** 185
- [66] Baxter R J 1977 *J. Stat. Phys.* **17** 1
- [67] Davies B 1988 *Physica A* **154** 1
- [68] Truong T T and Peschel I 1989 *Z. Physik B* **75** 119
- [69] Nienhuis B, Campostrini M and Calabrese P 2009 *J. Stat. Mech.* P02063
- [70] Eisler V, Legeza Ö and Rácz Z 2006 *J. Stat. Mech.* P11013
- [71] Iglói F and Juhász R 2008 *Europhys. Lett.* **81** 57003
- [72] Calabrese P and Cardy J L 2004 *J. Stat. Mech.* P06002

- [73] Franchini F, Its A R, Jin B-Q and Korepin V E 2007 *J. Phys. A: Math. Theor.* **40** 8467
- [74] Jin B Q and Korepin V E 2004 *J. Stat. Phys.* **116** 79
- [75] Keating J P and Mezzadri F 2004 *Comm. Math. Phys.* **252** 543
- [76] Sakai K and Satoh Y 2008 *J. High Energy Phys.* **12** 001
- [77] Levine G C and Miller D J 2008 *Phys. Rev. B* **77** 205119
- [78] Iglói F, Szatmári Z and Lin Y-C 2009 *Phys. Rev. B* **80** 024405
- [79] Eisler V, Iglói F and Peschel I 2009 *J. Stat. Mech.* P02011
- [80] Iglói F, Juhász R and Zimborás Z 2007 *Europhys. Lett.* **79** 37001
- [81] Lafflorencie N 2005 *Phys. Rev. B* **72** 140408
- [82] Iglói F, Lin Y-C, Rieger H and Monthus C 2007 *Phys. Rev. B* **76** 064421
- [83] Iglói F and Lin Y-C 2008 *J. Stat. Mech.* P06004
- [84] Keating J P, Mezzadri F and Novaes M 2006 *Phys. Rev. A* **74** 012311
- [85] Eisert J, Cramer M and Plenio M B 2009 *Rev. Mod. Phys.* to appear
- [86] Wolf M M 2006 *Phys. Rev. Lett.* **96** 010404
- [87] Gioev D and Klich I 2006 *Phys. Rev. Lett.* **96** 100503
- [88] Farkas S and Zimborás Z 2007 *J. Math. Phys.* **48** 102110
- [89] Li W, Ding L, Yu R, Roscilde T and Haas S 2006 *Phys. Rev. B* **74** 073103
- [90] Eisert J and Cramer M 2005 *Phys. Rev. A* **72** 042112
- [91] Peschel I and Zhao J 2005 *J. Stat. Mech.* P11002
- [92] Orus R, Latorre J I, Eisert J and Cramer M 2006 *Phys. Rev. A* **73** 060303
- [93] Zhou H Q, Barthel T, Fjærestad J O and Schollwöck U 2006 *Phys. Rev. A* **74** 050305(R)
- [94] Calabrese P and Cardy J L 2005 *J. Stat. Mech.* P04010
- [95] Bloch I, Dalibard J and Zwerger W 2008 *Rev. Mod. Phys.* **80** 885
- [96] Eisler V and Peschel I 2007 *J. Stat. Mech.* P06005
- [97] Bravyi S, Hastings M B and Verstraete F 2006 *Phys. Rev. Lett.* **97** 050401
- [98] Eisert J and Osborne T J 2006 *Phys. Rev. Lett.* **97** 150404
- [99] Fagotti M and Calabrese P 2008 *Phys. Rev. A* **78** 010306(R)
- [100] Rigol M, Muramatsu A and Olshanii M 2006 *Phys. Rev. A* **74** 053616
- [101] Cramer M, Dawson C M, Eisert J and Osborne T J 2008 *Phys. Rev. Lett.* **100** 030602
- [102] Barthel T and Schollwöck U 2008 *Phys. Rev. Lett.* **100** 100601
- [103] Calabrese P and Cardy J L 2007 *J. Stat. Mech.* P10004
- [104] Eisler V, Karevski D, Platini T and Peschel I 2008 *J. Stat. Mech.* P01023
- [105] Eisler V and Peschel I 2008 *Ann. Phys. (Berlin)* **17** 410
- [106] Barmettler P, Rey A M, Demler E, Lukin M D, Bloch I and Gritsev V 2008 *Phys. Rev. A* **78** 012330
- [107] Klich I and Levitov L 2009 *Phys. Rev. Lett.* **102** 100502
- [108] Harder G private communication
- [109] Cherng R W and Levitov L S 2006 *Phys. Rev. A* **73** 043614
- [110] Cincio L, Dziarmaga J, Rams M M and Zurek W H 2007 *Phys. Rev. A* **75** 052321